JOM, Vol. 68, No. 7, 2016
DOI: 10.1007/s11837-016-1937-7


# Manufacturing and Security Challenges in 3D Printing

STEVEN ERIC ZELTMANN,[1] NIKHIL GUPTA,[1,8] NEKTARIOS GEORGIOS TSOUTSOS,[2] MICHAIL MANIATAKOS,[3,6] JEYAVIJAYAN RAJENDRAN,[4] and RAMESH KARRI[5,7]

1.—Composite Materials and Mechanics Laboratory, Department of Mechanical and Aerospace Engineering, New York University Tandon School of Engineering, Brooklyn, NY 11201, USA. 2.—Department of Computer Science and Engineering, New York University Tandon School of Engineering, Brooklyn, NY 11201, USA. 3.—Engineering Division, New York University Abu Dhabi, Abu Dhabi, United Arab Emirates. 4.—Department of Electrical Engineering, University of Texas at Dallas, Richardson, TX 75080, USA. 5.—Department of Electrical and Computer Engineering, New York University Tandon School of Engineering, Brooklyn, NY 11201, USA. 6.—NYU Center for Cybersecurity, New York University Abu Dhabi, Abu Dhabi, United Arab Emirates. 7.—NYU Center for Cybersecurity, New York University Tandon School of Engineering, Brooklyn, NY 11201, USA. 8.—e-mail: ngupta@nyu.edu

As the manufacturing time, quality, and cost associated with additive manufacturing (AM) continue to improve, more and more businesses and consumers are adopting this technology. Some of the key benefits of AM include customizing products, localizing production and reducing logistics. Due to these and numerous other benefits, AM is enabling a globally distributed manufacturing process and supply chain spanning multiple parties, and hence raises concerns about the reliability of the manufactured product. In this work, we first present a brief overview of the potential risks that exist in the cyber-physical environment of additive manufacturing. We then evaluate the risks posed by two different classes of modifications to the AM process which are representative of the challenges that are unique to AM. The risks posed are examined through mechanical testing of objects with altered printing orientation and fine internal defects. Finite element analysis and ultrasonic inspection are also used to demonstrate the potential for decreased performance and for evading detection. The results highlight several scenarios, intentional or unintentional, that can affect the product quality and pose security challenges for the additive manufacturing supply chain.

## INTRODUCTION

Additive manufacturing (AM), or "3D printing*" is emerging as the next industrial revolution.[1] Polymer-based printing methods were the first to appear and have become an established prototyping and small-batch production technique.[2] Within the materials community, these techniques are experiencing a second wave as the technology evolves to incorporate highly optimized process control[3] and allow for printing using advanced materials.[4] AM is now used both in the prototyping and production phases, as seen in the prototype intake manifold and the injection molding die produced by Ford and displayed at the 2016 New York International Auto Show (Fig. 1). Detailed studies of the complete spectrum of properties are being evaluated for these material systems[5,6] subject to the unique process conditions in additive manufacturing. Fiber reinforced-[7,8] and nano-composites[9] are now also attainable in polymer 3D printers. Meanwhile, the field of metallic and ceramic AM is developing at a rapid pace.[10] Steel,[11] aluminum,[12] and titanium alloys[13,14] are being studied in depth for structural and medical implant applications. Selective laser sintering (SLS) and selective laser melting (SLM), the most commonly used processes for making metallic parts, involve progressively fusing a bed of metal powder using a high intensity laser. The complex interactions during high-temperature local

*Though the term "3D printing" traditionally referred only to deposition methods, we are following the popular trend to equate this term with AM.


(Published online May 11, 2016)

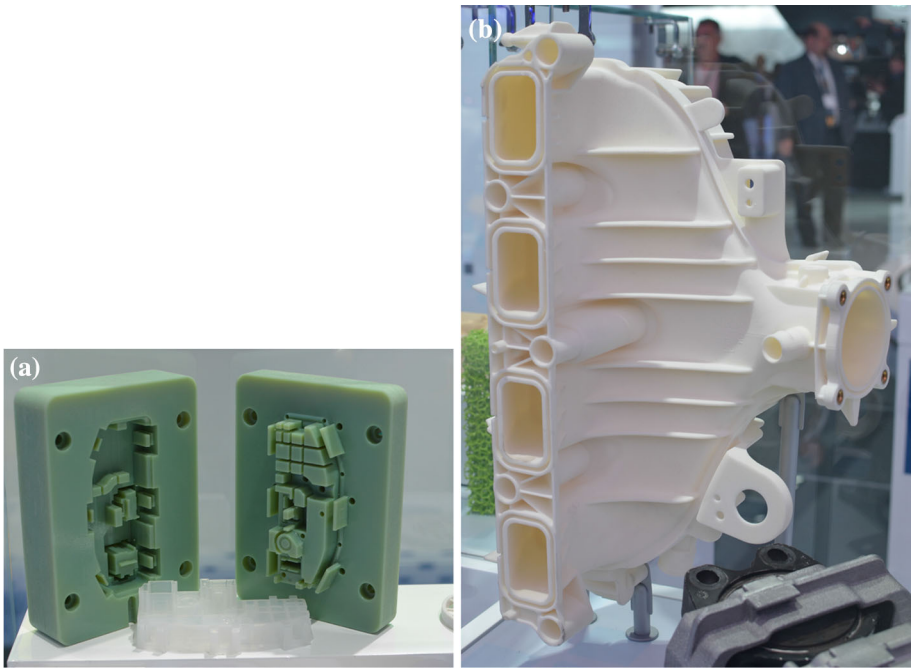


Fig. 1. (a) Injection molding dies and (b) prototype intake manifold produced by additive manufacturing and displayed by Ford at the 2016 New York International Auto Show.

sintering[15] can produce microstructural features (strong anisotropy, residual stresses, etc.) which make the design and analysis of such processes far more complex than their polymer counterparts. However, in some cases, the unique microstructure produced in these processes yields higher strength than in cast or wrought parts of the same alloy due to significant grain refinement[16] and possibility of in situ reinforcement.[17] The combination of exceptionally high properties and unlimited customizability has led to great interest in using AM metal components in medical implants, which has already become an accepted practice in the veterinary community,[18] and numerous companies are applying for Food and Drug Administration (FDA) certification for AM human implants.

For parts produced by material extrusion technology (also known as fused deposition modeling, or FDM), previous research has shown that unsuspecting AM operators could not distinguish between parts printed in different orientations.[19] Some work has also been done to address the applicability of traditional test methods to AM parts, and the necessary modifications to the standard procedures.[20,21] A goal of the present research is to propose a set of design and process rules that address the unique challenges introduced by AM to improve product performance and streamline the design process.

In this work, we investigate two manufacturing challenges that are unique to the AM process. First, we investigate the effect of sub-millimeter scale defects in the interior of 3D printed parts, as could be produced by contaminated feed material or machine errors. The size of the defects is on the order of print resolution of the printer. Second, we study the effect of the orientation of the part during printing on the material performance. Both are demonstrated on 3D-printed tensile test coupons and their impact is assessed using tensile testing. Ultrasonic non-destructive analysis is used to evaluate the ability to detect the defects, and finite element analysis is used to expand on the experimental study by evaluating the effect of defect size and location on the stress concentration.

## ADDITIVE MANUFACTURING PROCESS CHAIN

Figure 2 shows a typical AM process chain that includes computer-aided design, finite element analysis, and computer-controlled AM followed by testing and assembly. The following paragraphs elaborate on these important steps, with an eye towards the vulnerabilities present in each stage that could affect the final AM product.

### Design

This phase includes computer-aided design (CAD) and finite element analysis (FEA). A CAD team models the product based on the desired dimensions, properties and functionalities. The CAD software generates the 3D model of the object on which FEA is performed. The elastic properties of the material must be known beforehand in order to conduct the simulations, which will then guide revisions of the initial design until an optimal

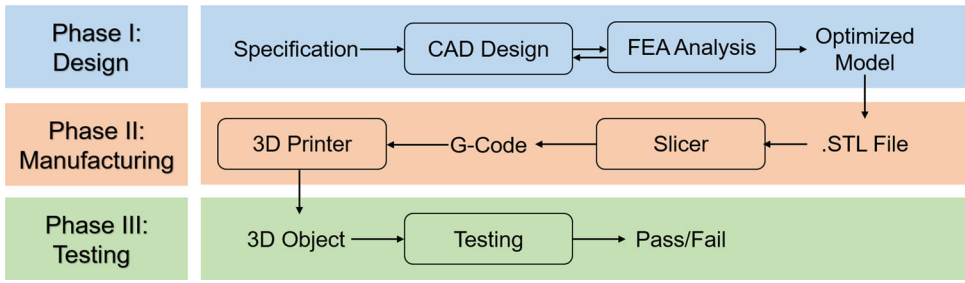


Fig. 2. Outline of additive manufacturing process chain.

design that meets all the requisite specifications is produced. One avenue opened by AM is an "adaptive" design process in which real-world usage data and FEA analysis are combined to continuously and semi-autonomously improve the functionality and reliability of the product.[22]

### Manufacturing

This phase includes slicing the 3D model and printing the object, and is where the AM process begins to diverge from traditional manufacturing. The final design of the object is converted to *.STL format,** which the slicer software then converts into a target-machine-specific tool path code; G-code is one standard format of such tool path code, though numerous proprietary formats are used by more sophisticated AM equipment. G-code (as applied to material extrusion machines) encodes the motion of the printer head along $x$, $y$, and $z$ directions, the amount of material to extrude, and the movement speed of the head. During this step, the G-code is loaded into the printer and the object is produced.

The slicing step (in material extrusion, SLA, etc.) also involves determining where to use support material and (in all techniques) how to position multiple models inside the print volume. When the printing step is conducted by an outside operator, economic use of the printer generally requires combining multiple parts or jobs into each machine run to maximize resource utilization. Ease of removal of the support material is also a major consideration in deciding printing orientation. However, this decision can significantly affect the performance of the final part, as will be demonstrated later in "Altered Printing Orientation".

### Testing

For quality control or validation, a prototype printed part may be subjected to mechanical and physical testing, which can be destructive or non-destructive (NDT). Depending on the uniqueness and required reliability of the parts, a randomly chosen sample or all of the produced parts may be inspected by NDT. Non-destructive testing methods include x-ray computed tomography (x-ray CT) and ultrasonic imaging, and vary greatly in terms of resolution and time investment. Destructive testing in the validation phase can include any of the common materials testing procedures or experiments designed to assess compliance with various government or industry standards. In simple AM components, this step is not much different than in traditional manufacturing, though increased part complexity may complicate such testing.

**Other formats are also available but *.STL format is currently by far the most widely used format.

## MATERIALS AND METHODS

### 3D Printing

#### *Embedded Defects*

The specimens with defects are printed using a Stratasys Connex500 (polymer material jetting type) printer with "Vero Clear" as the main material and "Tango Black Plus" as the contaminant. This printing system deposits a liquid photopolymer using a multi-jet head, curing the resin after each pass. The defect is created by jetting Tango material in place of Vero at the defect site. The test specimens are designed according to the tensile test geometry specified by the ASTM E8 standard.[23] Though the E8 standard is specified for testing of metallic specimens, it is used here so that the same STL files are used as in similar, ongoing experiments using SLS fabrication of steel specimens. The primary difference between the ASTM E8 Subsize specimens used here and the ASTM D638[24] standard used for polymers is the reduced radius of curvature in the shoulder (6 mm versus 12.7 mm). Specimens are printed with cubic defects of edge length 150 $\mu$m, 250 $\mu$m, and 500 $\mu$m, as well as without defect for control. All specimens are printed with the long axis along the $x$-direction of the printer bed. Defects smaller than 150 $\mu$m cannot be reliably printed using this technique due to the resolution limit of the system.

#### *Altered Printing Orientation*

The test specimens are printed with the same geometry, conforming to ASTM D638 standard. Slicing of the model is performed using Catalyst EX 4.4 software with the solid fill option and 0.01 inch (o.254 mm) layer height before printing using a Stratasys Dimension Elite FDM printer

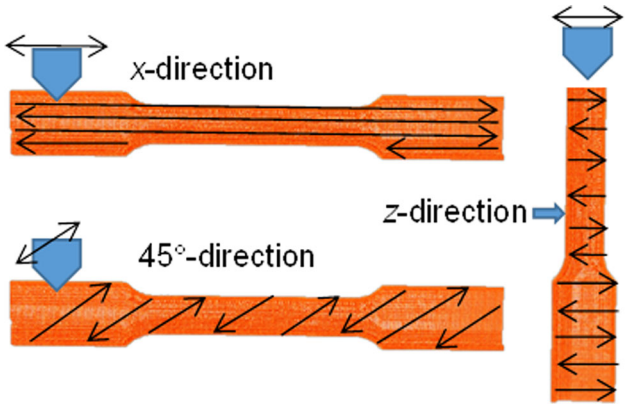


Fig. 3. Schematic of the orientations of specimens printed and tested for print direction alteration.

with Stratasys ABS*plus* material. Specimens are tested in three different orientations, which are termed here differently than the axis system of the printer. The $x$-orientation aligns the tool path with the long axis of the specimen, with the specimen laying flat on the print bed. The $+45^\circ$ direction is a rotation of the $x$-direction specimen about the $z$-axis, such that the tool path is inclined by $45^\circ$ with respect to the long axis, with the specimen laying flat on the bed. The $z$-orientation aligns the slices normal to the long axis, with the long axis aligned with the $z$-axis of the printer (the specimen stands on its end). The toolpath moves at $45^\circ$ to the edges of the slice. These directions are illustrated in Fig. 3. The tool changes direction by $90^\circ$ between subsequent layers. Hence, in each of the three cases, every other layer is oriented at $90^\circ$ to the primary direction described above.

## Characterization

### *Tensile Testing*

Tensile testing of the printed specimens is conducted using an Instron 4467 universal test frame with a 30-kN load cell and an Instron 1-inch (25.4 mm) gage length extensometer for strain measurement. A constant crosshead velocity is maintained with an initial strain rate of $10^{-3}$/s in the reduced section. Testing is continued until fracture of the specimen or 20% strain. The peak stress withstood by the specimen is taken as the tensile strength and the modulus is determined from the initial linear elastic region. Five specimens of each type are tested and the average values are presented.

### *Ultrasonic Inspection*

Non-destructive ultrasonic testing is performed using a Physical Acoustics Ultrapac 1000 ultrasonic scanner in C-scan mode with a 5-MHz transducer of 1 inch (25.4 mm) focal length. Pulse-echo mode is used with water coupling between the probe and the specimen. The time of flight and the amplitude are recorded during the tests. Separate specimens are used for ultrasonic inspection and tension testing. The specimens are printed in two perpendicular orientations to check the effect of surface texture direction on the visibility of the defect.

# RESULTS

## Embedded Defects

In this scenario, a specimen is printed with a small defect embedded at the center. The defect is created by printing a cubic feature of a soft elastomer-like polymer (Tango) within the test piece. The stiffness of the Tango material is significantly less than the Vero matrix, which mimics either a void inside the specimen or insertion of a nearly unattached foreign material. Both the severeness of the defect, in terms of reduction in any of the measures of mechanical performance, and the ability of the defect to be detected prior to service are studied. From the security perspective, it can be hypothesized that an internal or external rouge person may be motivated to create defects in the 3D-printed parts with the aim of compromising the product performance. They may consider small internal defects to be undetectable through the routine inspection. Such defects can be introduced by compromising solid models or by modifying the G-code. FEA conducted in this work will provide information on how the FEA results may change if the CAD files are compromised. The presence of defects may also be due to malfunctioning of the printer, problems with slicing leading to loss of information, or inconsistencies in the feed material properties.

### *Defect Detection*

The fabricated tensile test specimens are scanned using ultrasonic C-scan in order to determine whether a defect embedded in the part during printing can be detected by NDT inspection. The impedance of the elastomer-like defect will differ significantly from the stiff surrounding material, and may cause higher damping of the pulse. However, edge effects due to the small component size and the limited resolution of the technique may limit the ability to detect such defects.

The results of ultrasonic C-scans are shown in Fig. 4 for a non-defective specimen and a specimen with a 500 $\mu$m defect. The defect cannot be identified over the noise in the scan, so even the largest defect studied is effectively hidden. Identification of an internal defect depends on the defect size and location as well as the presence of other features that may mask the defect. The surface texture of the printed part causes artifacts which cannot be avoided. These artifacts dominate the scans of the test specimens. The different printing orientations of the two specimens are visible in the differing direction of the surface texture pattern. Changing

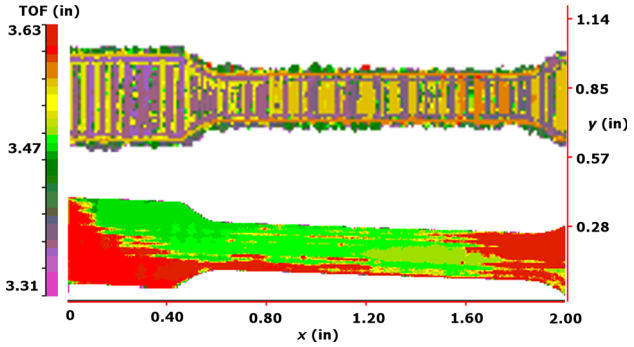


Fig. 4. Ultrasound C-scan images for specimens with no defect (top) and 500 $\mu$m defect (bottom). The time of flight is indicated on the color bar, and the position is marked on the bottom and right axes. The red-colored regions (darker regions in gray-scale image) near the specimens ends in the bottom figure are due to distortion of the specimen from clamping forces.

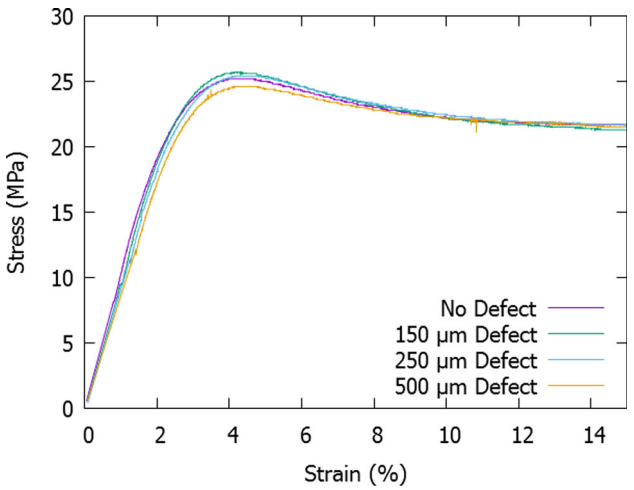


Fig. 5. Stress–strain curves for representative specimens with varying defect size.

the orientation was not observed to have any effect on the ability to detect the defect. Since the attenuation is higher in viscoelastic polymers compared to thermosets and metals, lower test frequencies must be used. Similar testing can be conducted in metallic specimens at 20 MHz frequency, which will significantly increase the resolution in the C-scan results.

*Tensile Testing*

A representative set of stress–strain curves from the tension testing of the specimens with varying defect size is shown in Fig. 5. The standard deviations (Table I) of the strength of each group of specimens overlaps and failure is found to initiate away from the center rather than at the defect. The specimens are observed to show ductile behavior, which minimizes the effect of the stress concentrations by allowing material around the defect to deform rather than initiate a crack.

*Finite Element Analysis*

In addition to physical testing, we conducted FEA simulations on the 3D models to demonstrate the impact of the defect and expand upon the experimental results. FEA is conducted using the commercial package Ansys 15.0. The elastic modulus and Poisson's ratio of the material are assigned as 2.2 GPa and 0.35 GPa, respectively, which corresponds to the manufacturer-specified values for Stratasys ABS*plus*. A convergence study is conducted in order to select the appropriate mesh size for all models and obtain results that are mesh-independent; convergence in displacement values is obtained. The FEA study involves simulating an "intact" tensile specimen to generate baseline properties, then observing the effect of embedding voids with different sizes and locations along the thickness.

A discretized model of an intact tensile test specimen is shown in Fig. 6a, where the specimen is constrained on one end and a force of 1 kN is applied at the other end. The specimens are modeled using isotropic materials, thus assuming no directionality in the material properties. The FEA simulation of the intact specimen (visualized in Fig. 6b) shows that that maximum von Mises stress obtained in this specimen geometry is 107.98 MPa and the location of the maximum is near the shoulder region. This is in agreement with the tension testing, where it was observed that the failure occurred away from the center of the gage section. On the other hand, the outer surface of a simulated model containing an internal defect is shown in Fig. 7. Compared to the intact specimen results, the location of maximum stress is no longer observed at the shoulder of the curvature in the defective models. Instead, the maximum stress is found inside the model, at the edge of the defect.

The FEA results for the specimens with embedded defects of various sizes at the center are shown in Fig. 8a–c. In comparison, Fig. 8d–f show the stress distribution when a same-size defect is moved to a different location along the specimen thickness. The simulation shows that the maximum stress occurs around the void, instead of on the shoulder as in the intact model. The values of maximum von Mises stress for the specimens having defects of different sizes and at different locations are compiled in Table II. The simulated stress for the intact model at the same location as the defect is 83 MPa, which indicates a shift in the location of the maximum stress point from the shoulder (intact model) to the defect point (defective model). For all defective specimens, the maximum observed von Mises stress is also higher than the value observed on the shoulder of the intact specimen (i.e., 107.98 MPa). For both depth locations (i.e., center and midway to surface), the stress concentration increases with the size of the defect (Table II).

**Table I. Experimental results for elastic modulus and strength for varying defect size**

| Defect size | Modulus (MPa) | Strength (MPa) |
|---|---|---|
| No defect | 976 ± 216 | 24.1 ± 4.6 |
| 150 $\mu$m | 1186 ± 285 | 29.9 ± 6.1 |
| 250 $\mu$m | 1287 ± 197 | 32.4 ± 5.4 |
| 500 $\mu$m | 937 ± 343 | 22.1 ± 4.4 |

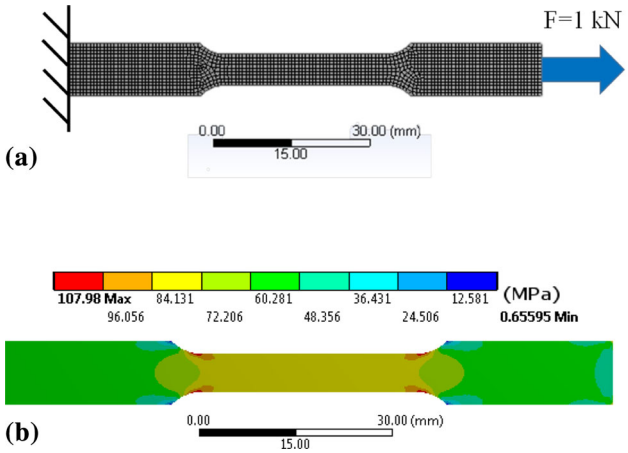


Fig. 6. (a) A meshed model and boundary conditions used in FEA. (b) FEA simulation of tension test on 3D-printed specimens with no defect. The maximum stress is on the shoulder region. The average stress in the reduced section is 83 MPa at the simulated load of 1 kN. This stress value is used as the nominal stress for finding the concentrations caused by the presence of a defect.

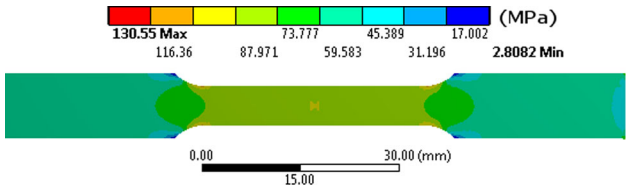


Fig. 7. Top view of the FEA results on a specimen with a 500 $\mu$m defect at 500 $\mu$m depth. A section view of the defect is shown in Fig. 8f.

## Altered Printing Orientation

In this scenario, we alter the tensile test specimen orientation with respect to the movement of the extrusion head. The preferred orientation is usually not specified to the AM operator and may not be at the customer's discretion in many commercial AM services. The tensile test experimental results for specimens printed in different directions are shown in Fig. 9, using five specimens in each orientation (in the interest of clarity only one specimen is included in the graph).

The tensile test results are presented in Table III. Compared to the $z$-direction orientation, the $x$ and 45° specimens have 36% and 15% higher modulus, respectively. In addition, the strength values of $x$ and 45° specimens are 28% and 30% higher, respectively, compared to the $z$-direction specimens. These results show that the 45° printing orientation is the best among the three directions. Thus, if the original model is intended to be oriented at 45° direction for printing, a change in the printing direction can significantly lower the strength and modulus, making the part underperform compared to the design conditions. Thermoplastic polymers contain long polymer chains, so the mechanical properties are dependent on their orientation. The feed wire is made by an extrusion process, which aligns the chains along the filament length. Depending on the process parameters, namely extrusion temperature and speed, this alignment can be retained along the toolpath direction.[25] The preferred orientation of polymer chains in the printed parts results may result in a change in strength and modulus with respect to the printing direction.

The ultrasonic results from the defect detection experiments presented in Fig. 4 show two specimens printed in different directions. Although the primary purpose of ultrasonic testing was to detect the presence of any defects present in the specimen, the surface texture could be resolved under the given test conditions to observe that the top specimen is printed in the $y$-direction and the bottom specimen is printed in the $x$-direction. The observed difference is only due to the surface roughness introduced in different directions. However, polishing, painting, and other surface treatments used on a final product would mask these features and prevent detection.

Among other parameters of interest is the failure strain. Figure 9 also shows that the failure strain is significantly compromised when the printing direction is changed. The 45° orientation provides over 8% strain before failure, while the other two orientations have less than 3% strain. Reduction in failure strain can reduce the response time available for intervention or repair and increases the possibility of catastrophic failure.

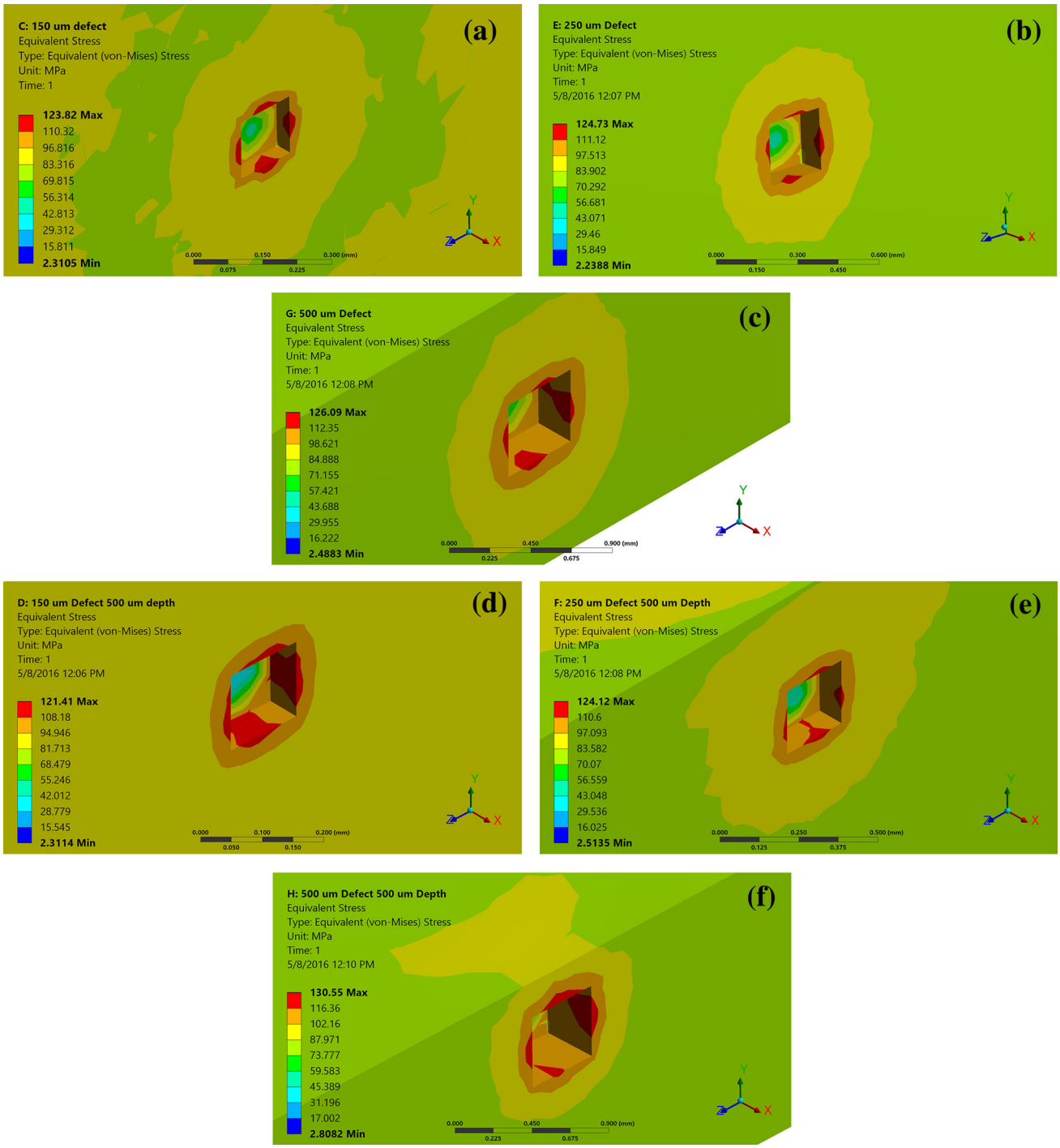


Fig. 8. FEA simulations of embedded defects in tensile bars. The stress distribution away from the defect is identical to that shown in Fig. 6b for the non-defective specimen. (a)–(c) Stress distribution for centrally placed defect size from 150 to 500 $\mu$m. (d)–(f) Stress distribution a defect placed midway between the center and the surface (same size ranges).

## DISCUSSION

### Embedded Defects

The photopolymer-based material jetting printing technique was chosen for producing test specimens because of the ability to reliably print small-sized features while using multiple materials. These features may be introduced by several reasons which include undesired features in the STL file due to the gaps caused by the tessellation process, printer skipping a print step due to mechanical issues, or a hacker intentionally introducing a sub-

**Table II. Maximum stress and stress concentration from FEA analysis**

| | Maximum stress (MPa) | | Stress concentration | |
|---|---|---|---|---|
| Defect size ($\mu$m) | 1 mm depth | 0.5 mm depth | 1 mm depth | 0.5 mm depth |
| 150 | 123.8 | 121.4 | 1.486 | 1.457 |
| 250 | 124.7 | 124.1 | 1.497 | 1.490 |
| 500 | 126.1 | 130.6 | 1.514 | 1.568 |

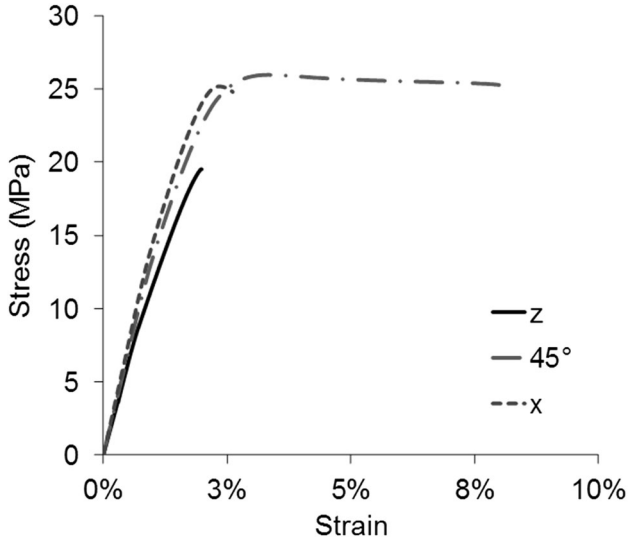


Fig. 9. Stress–strain curves for representative specimens fabricated in three different orientations.

**Table III. Experimental results for elastic modulus and strength for varying print orientation**

| Printing orientation | Modulus (GPa) | Strength (MPa) |
|---|---|---|
| 45° | 1.26 ± 0.13 | 25.70 ± 0.25 |
| *x* | 1.50 ± 0.10 | 25.19 ± 0.25 |
| *z* | 1.10 ± 0.13 | 19.75 ± 0.74 |

detection limit feature to compromise the product quality. The viscoelastic nature of these polymers means that high-resolution defect detection by ultrasound is generally infeasible. However, as the majority of photopolymers used in 3D printing are relatively ductile, it seems from these results that defects of this size scale (i.e., causing no significant reduction in load-bearing area) inside such parts is not a severe threat in this context. However, the photosensitive polymers used in material jetting are susceptible to embrittlement after exposure to elevated temperatures, moisture, or UV radiation. Brittle materials are more sensitive to the presence of defects than ductile materials. Therefore, such defective components may have lower fatigue life. In scenarios where 3D-printed metallic components are used under rigorous conditions, such as injection molding dies at high temperature and pressure for thousands of molding cycles, such defects may eventually cause premature failure due to damage accumulation around the stress concentration site.

Conversely, in material deposition techniques, the polymers used (ABS, PLA) are relatively more brittle. However, in such techniques, the resolution, ability to print with multiple materials, and ability to reliably create voids inside parts are more limited. Given these initial results, it appears that the presence of small defects will not have an appreciable effect on the performance of polymer parts. Further investigation may focus on inserting such defects in parts produced by selective laser sintering. The presence of unsintered powder inside the part, which could be caused by briefly interrupting the laser power during fabrication, by contaminated powder, or by clumping and uneven distribution of the powder, may evade ultrasonic and tomographic detection while causing an appreciable decrease in strength.

## Altered Printing Direction

The mechanical properties of the 3D-printed test coupons were found to be sensitive to the printing direction. This observation is significant from the perspective of component design, modeling, and production. Designers of components that are to be produced by AM must remain aware of this anisotropy and ensure that the orientations are communicated to the simulation and printing phases. In simple parts, such as the tensile coupons fabricated in this work, visual inspection itself may reveal the printing direction because the tool path is visible on the surface of material extrusion-produced components. However, in complex geometries, it may not be obvious to those handling the produced part that the correct orientation was chosen. In this work, we have only considered solid parts. Especially in material extrusion, material consumption and part weight are often substantially reduced by filling the interior of the part with a rectangular or hexagonal fill structure, which will have its cells aligned along the vertical axis of the printer regardless of part orientation. This can contribute significantly to the directionality of

behavior of the final part. These effects have also been documented in the literature for a variety of processes and materials.[26,27]

Previous research has shown many AM equipment operators do not normally notice the print orientation.[19] In the typical process chain, the operator of the printer selects the part orientation when inputting the *.STL file into the printer controller software. From the perspective of the operator, the optimal orientation of the part (in the absence of a clear directive from the design team) is the one that minimizes the use of support material and the footprint on the building platform to maximize the number of parts in one print operation. A simple recommendation would be to indicate the appearance of the tool path traces when the specified orientation is used in the specifications, thereby catching accidental and (crude) malicious alterations.

### Security Implications

Additive manufacturing is, by its definition, inextricably linked to the digital world.[28] The cyber-physical nature of AM raises important concerns: AM enables a globally distributed business model[29] wherein trusted, partially trusted and untrusted parties may be involved in the design and AM of a part.[30] Many AM machines are always connected to the network for possible remote queuing of jobs, diagnostics, and monitoring. This connectivity creates vulnerabilities and opens up possibilities of attack from external parties. Large-scale jobs may be outsourced to commercial 3D printing services, which may not be entirely trustworthy. Motivated by the inherent difficulty to validate trust in this emerging era of AM, where designs may be created by different parties but manufactured at any compatible printer, examination of the process chain must include consideration of these security concerns.

While these security concerns have not been widely discussed in the context of additive manufacturing, many of the concerns present in this system mirror those in the integrated circuit (IC) manufacturing chain. Processes that were once performed almost entirely in-house began to be outsourced to foreign third parties, which opened up numerous opportunities for piracy, counterfeiting, and insertion of trojans to cause early failure or to bypass encryption.[31] These risks have been extensively studied and numerous remedies are in place to improve security such as split manufacturing, where multiple parties manufacture separate aspects which each contain too little information to be of use, and obfuscation, where different logic gates are designed so as to be nearly indistinguishable from one another on the patterns used in manufacturing.[32] The security principles of this cyber-physical process chain can be used to inform the threat models and possible remedies in the additive manufacturing chain.

Malicious and deliberate modification of the print orientation or the introduction of defects are two possible attacks which may have devastating impact on the users of the final product and economic impact in the form of recalls and class action lawsuits. Lack of controls to preserve and monitor the integrity of a part from its conception and design to AM printing, as well as the need to destructively test samples to conclusively validate performance, allow for many potential exploits. As we have shown, defects may be introduced into the part which cannot be detected by typical NDT inspection. Alteration of the printing orientation can cause significant changes in the mechanical behavior which inspection of the part is also unable to detect.

These attacks are similar in spirit and execution to the hardware trojans seen in the IC process chain, and combating these attacks encounters the same challenge that untrusted parties necessarily must be provided with sufficiently detailed information to construct the part. However, the defenses against such attacks will likely be very different, because of the small-batch nature of AM as compared to the large production runs of ICs. Split manufacturing would remove the benefits of single-step production, as would obfuscation of macro-sized parts. Instead, solutions will likely focus on modifying the solid model files in such a way that conversion back to CAD representation is made more difficult, such as by splitting solid bodies or flat surfaces, while still preserving the same geometry when the slicer interprets it.

## CONCLUSION

In this work, we demonstrated some of the manufacturing challenges that arise in the cyber-physical ecosystem of the additive manufacturing process chain. In one demonstrated scenario, embedded defects in a 3D-printed specimen were found to be undetectable by ultrasonic inspection, though did not cause a decrease in the tensile strength. Such defects can still be detrimental under fatigue-loading conditions. FEA analysis indicated that such defects do indeed produce a stress concentration which, in other material systems, could lead to lower strength. In the other scenario, alteration of the direction of printing in the material extrusion process was shown to significantly alter the strength and strain to failure of the test specimens. Depending on the process and part complexity, alteration of the printing direction is difficult to detect and easily goes unnoticed. With the growth of cloud-based decentralized production environments enabled by the unique flexibility of additive manufacturing, it is critical that all entities

within the AM supply chain be aware of the unique challenges presented to avoid significant risk to the reliability of the product.

## ACKNOWLEDGEMENTS

The authors thank Fei Chen and Dr. Khalid Shahin for assistance with this work. The NYU-TSE Vice Dean for Research, Innovation, and Entrepreneurship, Dr. Kurt Becker, is thanked for providing an institutional fellowship to Fei Chen to contribute to this project. The authors acknowledge the Global Research Initiative Grant from NYU Abu Dhabi to Drs. Gupta and Shahin. Useful discussion with Dr. Dirk Lehmhus of IFAM, Germany is acknowledged. Parts of this work are supported by the Office of Naval Research Grant N00014-10-1-0988. The views and conclusions contained in this work are those of the authors and should not be interpreted as presenting the official policies or position, either expressed or implied, of the ONR or the U.S. Government unless so designated by other authorized documents. The proprietary and trade names mentioned are owned by their parent companies. Mention of any machines or products does not imply endorsement by the authors or funding agencies.

## REFERENCES

1. W. Gao, Y. Zhang, D. Ramanujan, K. Ramani, Y. Chen, C.B. Williams, C.C. Wang, Y.C. Shin, S. Zhang, and P.D. Zavattieri, *Comput. Aided Des.* 69, 65 (2015).
2. D. Lehmhus, T. Wuest, S. Wellsandt, S. Bosse, T. Kaihara, K.-D. Thoben, and M. Busse, *Sensors* 15, 32079 (2015).
3. S. Shaffer, K. Yang, J. Vargas, M.A.D. Prima, and W. Voit, *Polymer* 55, 5969 (2014).
4. M. Das, and V.K. Balla, in *Additive Manufacturing*, ed. by A. Bandyopadhyay, S. Bose (CRC Press, Boca Raton, 2015), pp. 297–326.
5. S.-H. Ahn, M. Montero, D. Odell, S. Roundy, and P.K. Wright, *Rapid Prototyp. J.* 8, 248 (2002).
6. J.P. Moore, and C.B. Williams, *Rapid Prototyp. J.* 21, 675 (2015).
7. A.R. Torrado, C.M. Shemelya, J.D. English, Y. Lin, R.B. Wicker, and D.A. Roberson, *Addit. Manuf.* 6, 16 (2015).
8. M. Sugavaneswaran and G. Arumaikkannu, *Mater. Des. A* 66, 29 (2015).
9. O. Ivanova, C. Williams, and T. Campbell, *Rapid Prototyp. J.* 19, 353 (2013).
10. N. Shamsaei, A. Yadollahi, L. Bian, and S.M. Thompson, *Addit. Manuf.* 8, 12 (2015).
11. T. Childs, C. Hauser, and M. Badrossamay, *Proc. Inst. Mech. Eng. B* 219, 339 (2005).
12. E. Louvis, P. Fox, and C.J. Sutcliffe, *J. Mater. Process. Technol.* 211, 275 (2011).
13. M. Seifi, M. Dahar, R. Aman, O. Harrysson, J. Beuth, and J. Lewandowski, *JOM* 67, 597 (2015).
14. H. Tang, M. Qian, N. Liu, X. Zhang, G. Yang, and J. Wang, *JOM* 67, 555 (2015).
15. P. Mercelis and J.-P. Kruth, *Rapid Prototyp. J.* 12, 254 (2006).
16. D. Zhang, Q. Cai, and J. Liu, *Mater. Manuf. Process.* 27, 1267 (2012).
17. D. Gu, Z. Wang, Y. Shen, Q. Li, and Y. Li, *Appl. Surf. Sci.* 255, 9230 (2009).
18. O. Harrysson, D. Marcellin-Little, and T. Horn, *JOM* 67, 647 (2015).
19. L.J. Wells, J.A. Camelio, C.B. Williams, and J. White, *Manuf. Lett.* 2, 74 (2014).
20. J. Slotwinski, A. Cooke, and S. Moylan, *NIST IR* (2012), p. 7847.
21. J. Slotwinski and S. Moylan, *NISTIR* (2014), p. 8005.
22. B.P. Conner, G.P. Manogharan, A.N. Martof, L.M. Rodomsky, C.M. Rodomsky, D.C. Jordan, and J.W. Limperos, *Addit. Manuf.* 14, 64 (2014).
23. ASTM E8–15a Standard Test Methods for Tension Testing of Metallic Materials, Tech. Rep. (ASTM International, West Conshohocken, 2015).
24. ASTM D638-14 Standard Test Method for Tensile Properties of Plastics (ASTM International, West Conshohocken, PA, 2014).
25. J.F. Rodrguez, J.P. Thomas, and J.E. Renaud, *Rapid Prototyp. J.* 7, 148 (2001).
26. B.E. Carroll, T.A. Palmer, and A.M. Beese, *Acta Mater.* 87, 309 (2015).
27. S. Ahn, M. Montero, D. Odell, S. Roundy, and P.K. Wright, *Rapid Prototyp. J.* 8, 248 (2002).
28. ASTM F2792–12a Standard Terminology for Additive Manufacturing Technologies, Tech. Rep. (ASTM International, West Conshohocken, 2012).
29. M. Bogers, R. Hadar, and A. Bilberg, *Technol. Forecast. Soc. Chang.* 102, 225 (2015).
30. L. Sturm, C. Williams, J. Camelio, J. White, and R. Parker, *Proceedings of International Solid Freeform Fabrication Symposium*, Austin, TX, (August 4–6, 2014), pp. 951–963.
31. R. Karri, J. Rajendran, K. Rosenfeld, and M. Tehranipoor, *Computer* 43, 39 (2010).
32. J. Rajendran, O. Sinanoglu, and R. Karri, *Design, Automation & Test in Europe Conference & Exhibition (DATE)*, Grenoble, France, (18–22 March, 2013), pp. 1259–1264.